Low-Complexity OSIC Equalization for OFDM-Based Vehicular Communications

Evangelos Vlachos, Aris S. Lalos, and Kostas Berberidis, *Senior Member, IEEE*

***Abstract*—Vehicular communication systems are usually equipped with orthogonal frequency division multiplexing (OFDM) transceivers that operate on rapidly changing radio propagation environments, which results in high Doppler and delay spreads. More specifically, in these environments, the experienced channels are doubly selective and introduce severe intercarrier interference (ICI) at the receiver. An effective ICI mitigation technique is desired as a constituent part of an ordered successive interference cancellation (OSIC) architecture, which turns out to be computationally efficient, since it may require the solution of linear systems with multiple right-hand sides. To decrease the complexity, several techniques suggest mitigating the ICI by considering only a small number of adjacent subcarriers. However, this approximation introduces an error floor, which may result in unacceptable bit error rates (BER) at high signal-to-noise ratio regimes. In this paper, we propose a new OSIC equalization technique based on an iterative Galerkin projection-based algorithm that reduces the computational cost without sacrificing the performance gains of the OSIC architecture. Furthermore, we suggest a new serial/parallel cancellation architecture that extends the OSIC and has the potential to completely cancel the experienced ICI introduced in high-mobility scenarios. Extensive Monte Carlo experiments have been carried out to validate the accuracy of our framework, revealing intriguing tradeoffs between achieved BER and complexity, and highlighting the importance of designing low-complexity OSIC schemes for OFDM systems operating over double selective channels.**

***Index Terms*—Gradient methods, interference cancellation, orthogonal frequency division multiplexing (OFDM), wireless access in vehicular, wireless communication.**

I. Introduction

A WIDELY employed technique for data communication in vehicular networks is the orthogonal frequency division multiplexing (OFDM) method. In OFDM systems, the inter-symbol interference (ISI) caused by the multipath environments is eliminated by dividing the entire channel into many narrow orthogonal subchannels. To maintain the orthogonality between subchannels, a cyclic prefix (CP) is inserted before each block of parallel data symbols. This property allows the use of single-tap equalizers in the frequency domain, offering a low computational cost that increases linearly with the number of subcarriers.

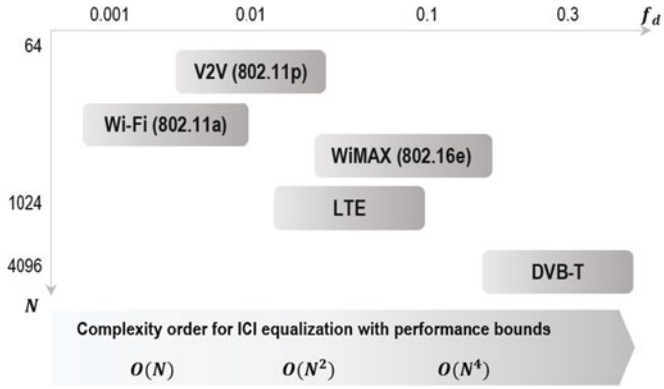

Fig. 1. Distribution of the wireless/mobile standards over the field of Doppler spread f_d and the subcarrier length N. Each standard is described by the minimum and the maximum possible normalized Doppler spread (f_d) that could be supported by using the lower and the higher defined carrier frequency, while the relative minimum and maximum speed was $v_{\min} = 100$ km/h and $v_{\max} = 350$ km/h. The complexity order characterization at the bottom has been obtained by constraining the maximum bit-error-rate (BER) at 10^{-3} with signa-to-noise-ratio (SNR) at 30 dB.

In applications with high levels of mobility, the experienced channels are usually both time and frequency selective (so-called *doubly selective*) [1]. The temporal variations within one OFDM block corrupt the subchannels orthogonality, generating power leakage among the subcarriers, and thus causing intercarrier interference (ICI) at the receiver [1], [2]. In these cases, single-tap equalization has been proved to be inadequate [3], [4], and thus advanced equalization techniques are usually employed in order to mitigate the ICI effect.

OFDM has been widely adopted by many communication standards in the Wi-Fi arena (e.g., WiFi (802.11a), V2V (802.11p) [5], and more) that defines an over-the-air interface between a wireless client and a base station or between two wireless clients. It has also been chosen for the cellular telecommunications standard LTE / LTE-A [6], and by other standards like WiMAX (802.16e) [7]. Moreover, it is the common modulation method for a number of broadcast standards from digital radio to the digital video broadcast standards (DVB-T/H [8]) and other broadcast systems as well, including digital radio Mondiale used for the long, medium, and short wave bands. In Fig. 1, we show a distribution of five mobile communication standards over the

Manuscript received October 9, 2014; revised December 27, 2015 and May 23, 2016; accepted July 7, 2016. Date of publication August 4, 2016; date of current version May 12, 2017. This work was supported in part by the University of Patras and by the European HANDiCAMS project under Grant 323944 under the Future and Emerging Technologies programme within the Seventh Framework Programme for Research of the European Commission. The review of this paper was coordinated by Dr. D. W. Matolak.

E. Vlachos and K. Berberidis are with the Department of Computer Engineering and Informatics, University of Patras, Patras 26504, Greece, and also with the Computer Technology Institute, Patras 26504, Greece (e-mail: vlaxose@ceid.upatras.gr; berberid@ceid.upatras.gr@ceid.upatras.gr).

A. S. Lalos is with the Department of Electrical and Computer Engineering, University of Patras, Patras 26504, Greece (e-mail: aris.lalos@ece.upatras.gr).

Color versions of one or more of the figures in this paper are available online at http://ieeexplore.ieee.org.

Digital Object Identifier 10.1109/TVT.2016.2598185

Doppler spread and the number of the subcarriers. In many cases in the aforementioned systems, the transceivers may experience high Doppler spreads, resulting in doubly selective channels that introduce severe ICI. This phenomenon is expected to be more apparent in milliliter wave communication systems that operate in much higher frequency bands (30 to 300 GHz) [9]. All the aforementioned facts have motivated system designers and researchers to focus on more complex equalization solutions that mitigate effectively the resulting ICI.

A. Related Work

Linear equalization (LE) [10], [11]; decision-feedback equalization (DFE) [12], [13]; and turbo equalization (TE) [14] schemes have been extensively studied as different techniques to mitigate the ICI. Stamoulis *et al.* [11] proposed a block linear minimum mean-square error (MMSE) equalizer architecture based on signal-to-interference noise (SINR) maximization criterion and then extended it to the multiple-input multiple-output (MIMO) OFDM case.

Choi *et al.* [12] presented an effective ICI cancellation equalizer that is based on ordered successive interference cancellation (OSIC). Specifically, the OSIC scheme works in an ordered successive manner for a given number of stages, where a symbol decision is made at each stage. The detected symbol is then removed from the input stream and is forwarded to the next stage. Although this scheme results into effective cancellation of severe ICI, it requires a prohibitively large number of operations, due to the solution of systems with multiple right-hand sides (RHS).

The complexity of the ICI equalizer may increase significantly with the number of subcarriers. To overcome this limitation, several authors suggest the use of approximation-based equalization techniques. In particular, the specific structure of the introduced ICI allows the development of equalizers that take into account the interference introduced by some adjacent subcarriers. Depending on the way that the mitigation process is executed, the equalizers are divided into *block* and *serial*. Block equalizers process the whole OFDM block simultaneously, whereas the serial ones consider each subcarrier separately, disregarding the effect of some nonadjacent subcarriers.

Suboptimal techniques for ICI equalization have been extensively studied in the literature, mainly due to their computational efficiency. For instance, banded ICI equalization techniques [10], [14]–[17] approximate the channel matrix with a banded one, exploiting its special structure. In [10] and [15] Jeon *et al.* proposed both LE and DFE schemes, that take into account the ICI introduced by a small number of subcarriers. Those schemes are quite attractive due to their low complexity but their performance in high-mobility scenarios degrades noticeably. Cai and Giannakis [13] first derived a matched-filter bound for OFDM systems operating over doubly selective channels and then proposed a MMSE DFE that outperforms the above equalizers without increasing significantly the required complexity. Moreover, TE schemes have been proposed in [14] and [18]. To be more specific, in [14], a turbo-like linear MMSE equalizer is proposed, where each symbol is iteratively estimated. In addition, the loglikelihood ratio is calculated for each estimated symbol and it is used as prior information for the detection of the next symbol. Fang *et al.* [18] also derived a turbo MMSE equalizer, which processes the whole OFDM block simultaneously, instead of considering the symbol loaded on each subcarrier separately, resulting in a computationally more efficient performance.

In order to obtain low-complexity techniques, several authors have proposed the employment of gradient-based optimization for zero forcing and MMSE equalization [19]–[22]. A time-domain equalizer based on an iterative method for solving the sparse linear equations is introduced in [19], termed as least squares with QR factorization (LSQR), which is then extended for ICI and ISI mitigation in [20]. In [22] and [21], a preconditioning structure for conjugate gradient (CG) has been proposed, which is suitable for OFDM systems with high Doppler spread.

At this point it should be noted that in high-mobility applications where OFDM systems experience severe ICI, all the approximation-based equalizers introduce an irreducible error floor that may result in unacceptable bit error rates (BER). This phenomenon becomes much more evident at high signal-to-noise ratio (SNR) regimes.

B. Contributions

In this paper, motivated by the aforementioned remarks, we focus on the nonbanded block OSIC equalization for ICI mitigation, and we propose a novel equalizer that employs a projections-based iterative algorithm for solving efficiently the multiple RHS systems. Specifically, the proposed method is based on the *Galerkin projections* (GP) [23] for solving the RHS exploiting an already formed Krylov subspace generated by the CG. For large OFDM blocks and depending on the predefined value for the termination parameter, the complexity order of the proposed iterative algorithm exhibits an order of magnitude lower complexity than the conventional OSIC technique [12].

In addition, a novel successive interference structure is proposed, that extends the OSIC architecture in this context. Specifically, we employ a parallel interference cancellation (PIC) within each successive stage to eliminate the forward along with the backward ICI in each subcarrier. The proposed architecture exhibits better performance to the OSIC without increasing the computational complexity significantly.

The proposed equalization method can be applied to any OFDM communication system operating over a double-selective channel. In particular, systems with severe ICI and quality-of-service (QoS) constraints can be significantly favored, i.e., WiMAX [7], LTE [6], DVB-H [8], and vehicle communications [5]. For instance, the safety related vehicle-to-vehicle (V2V) applications require a guaranteed QoS, but the ICI due to the fast-varying channel [24], challenges the reliability of communication. Moreover, MIMO V2V applications [25] may be characterized by large frame lengths, where the proposed equalizer could present significant practical benefits.

Organization of the Paper: The remainder of this paper is organized as follows: in Section II, the system model and the OSIC architecture are briefly reviewed. In Section III, after a short introduction to the GP-based iterative method, the proposed

algorithm along with the proposed successive interference cancellation (SIC)/PIC architecture are introduced. In Sections IV and V, the performance and the complexity of the proposed schemes are evaluated respectively, and finally, conclusions are drawn in Section VI.

Notation: Lower-(upper-)case boldface letters are reserved for column vectors (matrices); $(\cdot)^T, (\cdot)^H, (\cdot)^*$ denote the matrix transpose, complex conjugate transpose, and complex conjugate, respectively; $\mathcal{E}\{\cdot\}$ denotes the statistical mean operation; $\mathbf{F}$ and $\mathbf{F}^H$ denote the matrices for the discrete Fourier transform (DFT) and the inverse DFT respectively; $[A]_{i,j}$ denotes the component of the matrix $\mathbf{A}$ at the ith row and the jth column; $\delta(\cdot)$ denotes the Dirac's delta function; $\mathbf{0}_{M\times N}$ denotes a $M \times N$ matrix with zero components and $\mathbf{I}_N$ the $N \times N$ identity matrix; $\Pi(\cdot)$ denotes the hard decision operation; $\mathcal{C}(\cdot)$ denotes the circulant matrix of a vector.

II. Problem Formulation

A. System Model

Let us consider an OFDM system with N subcarriers operating over a time- and frequency-selective discrete-time baseband equivalent channel. A simplified block diagram of an OFDM transceiver, ignoring the units that perform sampling frequency estimation and carrier frequency offset estimation and mitigation, is depicted in Fig. 2. Let $\mathbf{s} = [\, s_1 \ \ldots \ s_N \,]^T \in \mathbb{C}^{N\times 1}$ be a set of N symbols at the output of the constellation mapper that are forwarded to the input of the inverse DFT (IDFT) unit. The s_k symbol is transmitted via the kth subcarrier. The output of the IDFT unit, denoted by $\mathbf{u} \triangleq \mathbf{F}^H\mathbf{s} \in \mathbb{C}^{N\times 1}$, is forwarded at the CP adder, where the time-domain OFDM symbol $\hat{\mathbf{u}} \in \mathbb{C}^{M\times 1}$ of length $M = N + N_{\text{cp}}$ is formed by adding a CP of length N_{cp} at the beginning of vector $\mathbf{s}$. This operation is described using the $M \times N$ matrix

$$\mathbf{C}^{\text{cp}} = \begin{bmatrix} \mathbf{0}_{N_{\text{cp}}\times(N-N_{\text{cp}})} & \mathbf{I}_{N_{\text{cp}}} \\ & \mathbf{I}_N \end{bmatrix} \tag{1}$$

so that $\hat{\mathbf{u}} \triangleq \mathbf{C}^{\text{cp}}\mathbf{s}$.

In wireless communications, a doubly selective fading channel is often modeled as a wide sense stationary uncorrelated scattering (WSSUS) channel [26]. In a discrete time model, the channel impulse response of this WSSUS channel can be expressed as $h(n,\tau) = \sum_{l=0}^{L-1} a(n,l)\delta(\tau - l)$, where $a(n,l)$ is complex zero mean Gaussian random variable. Assuming a causal channel with maximum delay spread $L \leq N_{\text{cp}}$, the received signal at the input of the OFDM demodulator may be written in vector form as

$$\mathbf{x} \triangleq \tilde{\mathbf{H}}_t\hat{\mathbf{u}} + \hat{\mathbf{w}} \tag{2}$$

where $\tilde{\mathbf{H}}_t \in \mathbb{C}^{M\times M}$ with $[\tilde{H}_t]_{i,j} = a\big(i, \text{mod}(i-j, L)\big)$ with $i, j \in 1, \ldots, M$, while $\text{mod}(\cdot, L)$ denotes the modulo-L: the operation. The vector $\hat{\mathbf{w}} \in \mathbb{C}^{M\times 1}$ represents the complex additive white Gaussian noise with $\hat{\mathbf{w}} \sim \mathcal{N}(0, \sigma^2\mathbf{I}_M)$. If we ignore the sampling and carrier frequency offset, the block of time-domain samples $\mathbf{x}$, passes through the CP removal unit of the OFDM demodulator, where the first N_{cp} samples are discarded. This operation may be written in vector form as

$$\mathbf{z} \triangleq \mathbf{R}^{\text{cp}}\mathbf{x} = \begin{bmatrix} \mathbf{0}_{N_{\text{cp}}\times N} & \mathbf{I}_N \end{bmatrix}\mathbf{x}. \tag{3}$$

Then, vector $\mathbf{z}$ passes through the DFT unit whose output is given by

$$\mathbf{y} \triangleq \mathbf{F}\mathbf{z} = \underbrace{\mathbf{F}\mathbf{R}^{\text{cp}}\tilde{\mathbf{H}}_t\mathbf{C}^{\text{cp}}\mathbf{F}^H}_{\mathbf{H}}\mathbf{s} + \mathbf{w} = \mathbf{H}\mathbf{s} + \mathbf{w} \tag{4}$$

where due to the unitary property of the DFT, the entries of $\mathbf{w}$ are complex Gaussian random variable with zero mean and variance σ^2.

If the involved channel is time invariant, i.e., $a_i(1) = a_i(2) = \cdots = a_i(N)$, $i = 1, \ldots, L$, the matrix $\mathbf{H}$ becomes diagonal since $\mathbf{R}^{\text{cp}}\tilde{\mathbf{H}}_t\mathbf{C}^{\text{cp}}$ has a circulant structure, and therefore, equalization is possible with computational complexity cost $\mathcal{O}(N)$. On the contrary, in case the channel is time varying, the matrix $\mathbf{H}$ is no longer diagonal due to the introduced ICI, and hence, nontrivial equalization techniques are required.

B. Ordered Successive Interference Cancellation

In this section, we provide a short overview of the OSIC architecture, which offers an effective ICI reduction as compared with linear equalization with the cost of higher complexity. The results that are presented here will form the basis for the new technique that will be derived in Section III.

To comprehend the basic idea, let us first recall that each subcarrier is related with one of the N transmitted data symbols. Thus, OSIC architecture is comprised by N *stages*, where at each stage we can easily subtract the part of the ICI that is associated with the decisions already made at previous stages. Specifically, assuming that the symbols are detected successively in the order $s_{z_1}, s_{z_2}, \ldots, s_{z_N}$, then at the kth stage, we seek for the MMSE minimizer, which is expressed as

$$\mathbf{g}_{z_k} = \arg\min_{\mathbf{g}_{z_k}} \frac{1}{2}\mathcal{E}\{|\mathbf{g}_{z_k}^H\mathbf{y}_{z_k} - s_{z_k}|^2\}, \ k = 1, \ldots, N \tag{5}$$

where $\mathbf{g}_{z_k}$ denotes the equalizer filter of the k stage, and $\mathbf{y}_{z_k}$ is the updated vector of the received OFDM block after the cancellation of $k-1$ previously detected symbols, with $\mathbf{y}_{z_1} \triangleq \mathbf{y}$.

Equivalently, (5) is expressed as the solution of the following system of equations:

$$\big(\mathbf{H}_{z_k}^H\mathbf{H}_{z_k} + \sigma^2\mathbf{I}_{N-k+1}\big)\,\mathbf{g}_{z_k} = \mathbf{h}_{z_k} \tag{6}$$

where $\mathbf{h}_{z_k}$ is the z_kth column of the channel matrix $\mathbf{H}_{z_k}^H$, and $\mathbf{H}_{z_k}$ denotes the channel matrix after the removal of the $k-1$ columns $\{\mathbf{h}_{z_1}, \ldots, \mathbf{h}_{z_{k-1}}\}$, with $\mathbf{H}_{z_1} \triangleq \mathbf{H}$.

Provided that we have reached to the solution of the system (6) (either via matrix inversion or via iterative algorithm), the detection of the current symbol is expressed as

$$\hat{s}_{z_k} = \Pi(\mathbf{g}_{z_k}^H\mathbf{y}_{z_k}). \tag{7}$$

The symbol decision $\hat{s}_{z_k}$ is then used to provide an estimate of the respective ICI, that is, $\mathbf{h}_{z_k}\hat{s}_{z_k}$, which in the next stage z_{k+1}, it will have been subtracted from the received OFDM block, i.e.,

$$\mathbf{y}_{z_{k+1}} = \mathbf{y}_{z_k} - \mathbf{h}_{z_k}\hat{s}_{z_k} \tag{8}$$

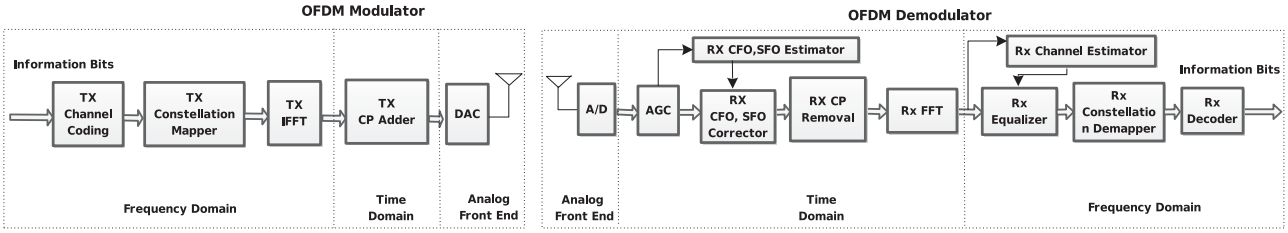

Fig. 2. OFDM block diagram.

and the procedure continues likewise for the next subcarrier symbol $s_{z_{k+1}}$. Since this architecture resembles that of a decision-feedback equalizer [27], one can expect an error propagation phenomenon. However, assuming that $\hat{s}_{z_k}$ has been correctly detected, its interference will be canceled from the subsequent stages.

It is well-known that the detection order in OSIC architecture has significant impact in the performance of the equalizer [27], [28]. Typically, the optimal detection order can be obtained by maximizing the SINR at the receiver, since it is known that the maximization of the SINR also minimizes the achievable BER in an OFDM system [29]. Hence, at each stage k, we have that

$$z_k = \arg\max_{l} \frac{|\mathbf{g}_l^H \mathbf{h}_l|^2}{\sum_{m\neq k}^{m} |\mathbf{g}_l^H \mathbf{h}_m|^2 + \sigma \|\mathbf{g}_l\|_2^2}$$
$$\forall l \in [z_{k+1}, z_{k+2}, \ldots, z_N]. \tag{9}$$

It is important to note that, the computation of SINR at the stage z_k, requires the knowledge of $\mathbf{g}_{z_{k+1}}, \ldots, \mathbf{g}_{z_N}$ equalization vectors, which are obtained from the solution of the following systems:

$$\left(\mathbf{H}_{z_k}^H \mathbf{H}_{z_k} + \sigma^2 \mathbf{I}_{N-k+1}\right) \mathbf{g}_l = \mathbf{h}_l, \quad \text{with } l \in [z_{k+1}, z_N] \tag{10}$$

where the autocorrelation matrix is same for all the RHS since it is updated once per stage.

Concatenating the equalization vectors of the current stage z_k and the subsequent stages $z_{k+1}, \ldots, z_N$, into the matrix $\mathbf{G}_{z_k} = [\mathbf{g}_{z_k} \mathbf{g}_{z_{k+1}} \cdots \mathbf{g}_{z_N}]^T \in \mathbb{C}^{N-k\times N}$, then at each stage, the solution of the following system with N RHS is obtained by solving the following system:

$$\left(\mathbf{H}_{z_k}^H \mathbf{H}_{z_k} + \sigma^2 \mathbf{I}_{N-k+1}\right) \mathbf{G}_{z_k} = \mathbf{H}_{z_k}^H. \tag{11}$$

III. Proposed Equalizer

In this section, first we provide a preliminary discussion for the GP technique that is employed for the efficient solution of systems of equations with multiple RHS. Afterward, we describe the proposed techniques for OSIC equalization that exploit the GP. Finally, the proposed serial/parallel ICI architecture is introduced.

A. Preliminaries: Galerkin Projections

To reduce the computational cost of the direct method, approximate solutions through iterative techniques are usually employed. It is known that the so-called *Krylov subspace methods* [30]–[32] (i.e., steepest descent, CG, and LSQR) can be used to efficiently solve the linear system of equations.

In the case of block MMSE for ICI equalization, one must compute the equalization matrix $\mathbf{G} \in \mathbb{C}^{N\times N}$ via the solution of the system of equations with multiple RHS, $\left(\mathbf{H}^H\mathbf{H} + \sigma^2\mathbf{I}_N\right)\mathbf{G} = \mathbf{H}$, where $\mathbf{H} \in \mathbb{C}^{N\times N}$; afterward, the soft-decisions vector must be obtained, given by $\tilde{\mathbf{s}} = \mathbf{G}\mathbf{y} \in \mathbb{C}^{N\times N}$. Since MMSE equalization turns into finding a solution of a linear system, where the matrix is Hermitian and positive definite, the CG algorithm is more suitable from other Krylov subspace methods.

The straightforward application of CG for solving the multiple RHS (10) in N stages would require a complexity of $\mathcal{O}(N^4 I)$ complex operations, where $I = \sum_{k=1}^{N} I_k$ and I_k denotes the total iterations and the kth stage iterations, respectively, required for the convergence. In particular, let us denote by $\mathcal{C}_{\text{cg}}^{\text{conv}}$ the complexity of the conventional technique, then

$$\mathcal{C}_{\text{cg}}^{\text{conv}} = \underbrace{\underbrace{\sum_{k=0}^{N-1} \underbrace{\sum_{l=k}^{N-1} \underbrace{\sum_{i=1}^{I_k} \mathcal{O}\left((N-k)^2\right)}_{\text{CG iterations}}}_{\text{multiple RHS}}}_{\text{stages}}} \tag{12}$$

where the outer sum represents the total complexity for the computation of the $N \times N$ equalizer matrix (with the kth column vector representing the equalizer at the kth stage), the middle sum represents the complexity for the remaining RHS at the kth stage, and the inner sum represents the complexity of the CG algorithm that runs for a predefined number of iterations I_k.

A more sophisticated approach for iterative approximation of systems with multiple RHS has been suggested in the literature, known as GP [17], [23], [33], [34]. The main idea of this technique is to exploit an already generated Krylov subspace for the solution of more than one system. Recall that the construction of the Krylov subspace is the most costly step of the CG algorithm. Therefore, through low-cost projections on the generated subspace, approximated solutions of the unsolved RHS can be obtained.

Originally, in [23] and [33], the approximated solutions given by the projections are used as initialization vectors for the CG procedure since proper initialization of the CG algorithm provides one way to reduce complexity without sacrificing estimation accuracy. According to the GP methodology, the multiple RHS system is decomposed into two parts: the *seed* system and the *nonseed* systems. The seed system, is solved iteratively via

the CG algorithm, where the solution vector is expressed as a linear combination of the Krylov subspace basis components. Afterward, the solution vectors of the remaining nonseed systems can be approximated based on projections onto the already generated Krylov subspace. This procedure continues until all the systems have been selected as a seed once. The described procedure of selecting a new seed is termed as *restart*.

Here let us note that the order of the seed selection is obtained in a lexicographic manner. The complexity order of the algorithm is given by $\mathcal{C}_{\text{cggp}} = \sum_{k=0}^{N-1} \sum_{i=1}^{I_k} \mathcal{O}\left((N-k)^2\right)$, where I_k is the number of algorithm's iterations required for the convergence of the kth system. From the perspective of complexity minimization, the value of I_k must be determined based on the approximation error at each iteration, rather than defined *a priori*. In that case, fast convergence to the solution implies low computational complexity. In [23], it was proven that, by using GP as initialization, a very small number of restarts is required for the convergence of all the RHS, indicating super-linear convergence behavior.

B. Proposed Algorithm

Let us here describe the proposed iterative algorithm, which can be used for efficiently computing the equalizer at the z_k-stage of the OSIC, i.e.,

$$\mathbf{A}_{z_k}\mathbf{G} = \mathbf{H}_{z_k}^H \tag{13}$$

where $\mathbf{A}_{z_k} \triangleq \left(\mathbf{H}_{z_k}^H \mathbf{H}_{z_k} + \sigma^2 \mathbf{I}_{N-k+1}\right)$, and for brevity we have removed the stage indexing from the equalizer matrix $\mathbf{G}$. Let the mth system be the seed, then at the ith CG iteration, a basis of the Krylov subspace will have been formed as $\mathcal{K}_{m,i} = \text{span}\{\mathbf{d}_m^0, \mathbf{d}_m^1, \ldots, \mathbf{d}_m^{i-1}\}$, where $\mathbf{d}_m^\ell$ is the search direction of the mth system at the ℓth iteration, and span$\{\cdot\}$ denotes the generating function of all linear combinations of the vectors $\mathbf{d}_m^\ell$ for $\ell = 0, 1, \ldots, i-1$ [30]. After at most N iterations, the obtained solution $\mathbf{g}_m \triangleq \mathbf{g}_m^N$ minimizes the associated quadratic functional $\mathcal{J}$ with respect to $\mathbf{g}_m$, i.e.,

$$\mathcal{J}(\mathbf{g}_m) = \frac{1}{2}\mathbf{g}_m^H \mathbf{A}_{z_k}\mathbf{g}_k - \mathbf{h}_m^H \mathbf{g}_m. \tag{14}$$

According to the well-known CG procedure, the search direction $\mathbf{d}_m^i$ is constructed by applying the ith step of the Gram–Schmidt procedure to the residual vector $\mathbf{r}_m^i = -\nabla\mathcal{J}(\mathbf{g}_m^i) = \mathbf{h}_m - \mathbf{A}_{z_k}\mathbf{g}_m^i$ and the preceding directions $\mathbf{d}_m^0, \mathbf{d}_m^1, \ldots, \mathbf{d}_m^{i-1}$. Taking into account that the gradient $\nabla\mathcal{J}(\mathbf{g}_m^i)$ is orthogonal to the subspace spanned by the previous directions, we get

$$\mathbf{d}_m^i = \mathbf{r}_m^i + \beta^i \mathbf{d}_m^{i-1} \tag{15}$$

where $\beta^i = \frac{(\mathbf{r}_m^i)^H \mathbf{r}_m^i}{(\mathbf{r}_m^{i-1})^H \mathbf{r}_m^{i-1}}$. For the given set of i $\mathbf{A}$-conjugate directions, the approximate solution $\mathbf{g}_m^i$ can be expressed as a linear combination of the already estimated directions as follows:

$$\mathbf{g}_m^i = \alpha^0 \mathbf{d}_m^0 + \cdots + \alpha^i \mathbf{d}_m^i = \mathbf{x}_m^{i-1} + \alpha^i \mathbf{d}_m^i \tag{16}$$

where the step-size α^i is obtained via line minimization as $\alpha^i = \frac{(\mathbf{r}_m^i)^H \mathbf{r}_m^i}{(\mathbf{d}_m^i)^H \mathbf{A}_{z_k} \mathbf{d}_m^i}$. Based on (16), the residual vector for the ith iteration can be expressed as $\mathbf{r}_m^i = \mathbf{r}_m^{i-1} - \alpha^i \mathbf{A}_{z_k}\mathbf{d}_m^i$.

Algorithm 1: Galerkin projections-based CG algorithm (multiple-seed version) for the k-th SIC stage.

Data: $\mathbf{A}_{z_k}$, $\mathbf{H}_{z_k}$, $\mathbf{G}^0$
Result: $\mathbf{G}$

1 Initialization: $\mathbf{R}^0 = \mathbf{H}_{z_k} - \mathbf{A}_{z_k}\mathbf{G}^0$
2 **for** $m = 1, 2, \ldots, N-k+1$ **do**
3 $i \longleftarrow 0$
4 **while** $\|\mathbf{r}_m^{i-1}\| < \epsilon$ **do**
5 $\rho^i \longleftarrow \|\mathbf{r}_m^{i-1}\|$
6 **if** $i = 0$ **then**
7 $\mathbf{d}_m^i \longleftarrow \mathbf{r}_m^{i-1}$
8 **else**
9 $\beta^i \longleftarrow \rho^i / \rho^{i-1}$
10 $\mathbf{d}_m^i \longleftarrow \mathbf{r}_m^{i-1} + \beta^i \mathbf{d}_m^{i-1}$
11 $\boldsymbol{\mathcal{V}}^i \longleftarrow \mathbf{A}_{z_k}\mathbf{d}_m^i$
12 $\mathcal{C}^i \longleftarrow (\mathbf{d}_m^i)^H \boldsymbol{\mathcal{V}}^i$
13 $\alpha^i \longleftarrow \rho^i / \mathcal{C}^i$
14 $\mathbf{g}_m^i \longleftarrow \mathbf{g}_m^{i-1} + \alpha^i \mathbf{d}_m^i$
15 $\mathbf{r}_m^i \longleftarrow \mathbf{r}_m^{i-1} - \alpha^i \boldsymbol{\mathcal{V}}^i$
16 **for** $\ell = m+1, \ldots, N$ **do**
17 $\zeta^i \longleftarrow (\mathbf{d}_m^i)^H \mathbf{r}_\ell^{i-1} / \mathcal{C}^i$
18 $\mathbf{g}_\ell^i \longleftarrow \mathbf{g}_\ell^{i-1} + \zeta^i \mathbf{d}_m^i$
19 $\mathbf{r}_\ell^i \longleftarrow \mathbf{r}_\ell^{i-1} - \zeta^i \boldsymbol{\mathcal{V}}^i$
20 $i \longleftarrow i + 1$

Considering the nonseed systems, i.e., the remaining $N-1$ RHS

$$\mathbf{A}_{z_k}\mathbf{g}_l = \mathbf{h}_l^H, \quad \text{with } l \in [2, \ldots, N] \tag{17}$$

the approximate solutions are obtained by solving the minimization problems $\min_\alpha \mathcal{J}(\mathbf{g}_l^i + \alpha \mathbf{d}_m^i)$ for all l. Note that, the search direction vector $\mathbf{d}_m^i$ has already been generated from the ith iteration of the seed system. The update rule for the solution vector is expressed as

$$\mathbf{g}_l^i = \mathbf{g}_l^{i-1} + \alpha^l \mathbf{d}_m^i \tag{18}$$

where $\alpha^l = \frac{(\mathbf{d}_m^i)^H \mathbf{r}_l^{i-1}}{(\mathbf{d}_m^i)^H \mathbf{A}_{z_k}^H \mathbf{d}_m^i}$ and $\mathbf{r}_l^{i-1}$ is the residual of the lth system at the $i-1$ iteration that is updated according to

$$\mathbf{r}_l^i = \mathbf{r}_l^{i-1} - \alpha^l \mathbf{A}_{z_k}^H \mathbf{d}_m^i. \tag{19}$$

Note that the quantity $\mathbf{A}_{z_k}^H \mathbf{d}_m^i$ has already been computed at the ith iteration of the seed system.

The described procedure is shown in Algorithm 1. The "for" loop at line 2 represents the restarts, whereas the termination criterion is at line 4. At lines 5–16, the GP steps are listed, which are followed by the projections procedure at lines 17–21. The costly parts of the algorithm are the matrix vector products at lines 12 and 18.

1) Performance/Complexity Tradeoff: The termination criterion of Algorithm 1 is defined by the value of the parameter ϵ, which determines the tradeoff between the performance and the complexity of the method. In the following, we provide a relation between the parameter ϵ, which is a user-defined

parameter, and the reconstruction error of the algorithm, which is defined as $\zeta \triangleq \|\mathbf{g}_m^{\star} - \mathbf{g}_m^I\|$.

Given that I denotes the maximum number of iterations for the m-system in Algorithm 1, then the error residual vector is given by

$$\mathbf{r}_m^I = \mathbf{b}_m - \mathbf{R}_m \mathbf{g}_m^I = \mathbf{A}_{z_k} \mathbf{g}_m^{\star} - \mathbf{A}_{z_k} \mathbf{g}_m^I = \mathbf{A}_{z_k} \left(\mathbf{g}_m^{\star} - \mathbf{g}_m^I\right) \tag{20}$$

where $\mathbf{g}_m^{\star}$ is the equalizer vector computed via matrix inversion in (6). Then, the norm of the error residual can be bounded according to the following expression:

$$\|\mathbf{r}_m^I\| < \|\mathbf{A}_{z_k}\| \|\mathbf{g}_m^{\star} - \mathbf{g}_m^I\| = \|\mathbf{A}_{z_k}\| \zeta. \tag{21}$$

To proceed, note that $\|\mathbf{A}_{z_k}\| = \|\mathbf{H}_{z_k}^H \mathbf{H}_{z_k} + \sigma^2 \mathbf{I}\| < \|\mathbf{H}_{z_k}^H \mathbf{H}_{z_k}\| + \sigma^2 < \|\mathbf{H}_{z_k}\|^2 + \sigma^2$. Since $\mathbf{H}_{z_k}$ has $k-1$ fewer columns than $\mathbf{H}_{z_1}$, we have that $\|\mathbf{H}_{z_k}\| < \|\mathbf{H}\|$, hence we have that $\|\mathbf{A}_{z_k}\| < \|\mathbf{H}\|^2 + \sigma^2$. Therefore, the residual error is upper bounded by

$$\|\mathbf{r}_m^I\| < \left(\|\mathbf{H}\|^2 + \sigma^2\right) \zeta \triangleq \epsilon \tag{22}$$

i.e., ϵ represents the normalized reconstruction error. Equation (22) provides us with the termination criterion based on the reconstruction error. Let us note here that, the value of the parameter ϵ has a direct impact on the maximum number of iterations that are required for convergence. In particular, a small value would result into small reconstruction error and also to a high number of iterations ($I \to N$), which are required in order to reach the desired accuracy. On the contrary, a large value for ϵ would result into worse accuracy and fewer iterations ($I \ll N$).

C. Single-Seed Version

The fact that a very small number of restarts is usually required for the convergence of all the RHS, motivated us to propose the single-seed approximation, i.e., $M = 1$. However, it should be noted that a direct application of $M = 1$ to the Algorithm 1 would suffer from large approximation error, as it will be justified in the rest part of this paper. For this reason, we consider the equivalent transposed system of equations, i.e.,

$$\left(\mathbf{H}_{z_k} \mathbf{H}_{z_k}^H + \sigma^2 \mathbf{I}_N\right) \mathbf{G}_{z_k} = \mathbf{H}_{z_k}. \tag{23}$$

In this case, the size of the systems remains the same, whereas the number of the RHS is decreased by one. It is important to note that, the reduction of the RHS at each stage, enables a more meaningful connection between the stages and the RHS, i.e., each RHS corresponds to a specific stage.

The seed system is solved by the CG algorithm obtaining a high accuracy solution, whereas the nonseed systems are solved by the GP procedure approximating closely the true solutions. However, since the nonseed systems will be used only for the ordering step of OSIC equalizer, this approximation scheme will have a smaller impact to the overall performance. In Table I, we illustrate this idea, where at each position the term CG or GP is used to indicate the method that is used to approximate the equalization vector.

The described procedure is shown in Algorithm 2. Note that the projection procedure, listed in lines 16–20, is conducted for $N - k + 1$ systems.

TABLE I
ALLOCATION OF THE CG AND GP METHODS, FOR THE SINGLE-SEED VERSION

Stage index ↓ / Subcarrier index ⟶	1st	2nd	3rd	4th	…	Nth
z_1	**CG**	*GP*	*GP*	*GP*	…	*GP*
z_2	–	**CG**	*GP*	*GP*	…	*GP*
⋮	⋮	⋮	⋮	⋮	⋮	
z_N	–	–	–	–	–	**CG**

Algorithm 2: Galerkin projections-based CG algorithm (single-seed version) for the k-th SIC stage.

Data: $\mathbf{A}_{z_k}$, $\mathbf{H}_{z_k}$, $\mathbf{G}^0$
Result: $\mathbf{G}_{z_k}$
1 Initialization: $\mathbf{R}^0 = \mathbf{H}_{z_k} - \mathbf{A}_{z_k}\mathbf{G}^0$
2 $i \longleftarrow 0$
3 **while** $\|\mathbf{r}_1^{i-1}\| < \epsilon$ **do**
4 $\quad \rho^i \longleftarrow \|\mathbf{r}_1^{i-1}\|$
5 $\quad$ **if** $i = 0$ **then**
6 $\quad\quad \mathbf{d}_1^i \longleftarrow \mathbf{r}_1^{i-1}$
7 $\quad$ **else**
8 $\quad\quad \beta^i \longleftarrow \rho^i / \rho^{i-1}$
9 $\quad\quad \mathbf{d}_1^i \longleftarrow \mathbf{r}_1^{i-1} + \beta^i \mathbf{d}_1^{i-1}$
10 $\quad \boldsymbol{\mathcal{V}}^i \longleftarrow \mathbf{A}_{z_k}\mathbf{d}_1^i$
11 $\quad \mathcal{C}^i \longleftarrow (\mathbf{d}_1^i)^H \boldsymbol{\mathcal{V}}^i$
12 $\quad \alpha^i \longleftarrow \rho^i / \mathcal{C}^i$
13 $\quad \mathbf{g}_1^i \longleftarrow \mathbf{g}_1^{i-1} + \alpha^i \mathbf{d}_1^i$
14 $\quad \mathbf{r}_1^i \longleftarrow \mathbf{r}_1^{i-1} - \alpha^i \boldsymbol{\mathcal{V}}^i$
15 $\quad$ **for** $\ell = 2, \ldots, N - k + 1$ **do**
16 $\quad\quad \zeta^i \longleftarrow (\mathbf{d}_1^i)^H \mathbf{r}_\ell^{i-1} / \mathcal{C}^i$
17 $\quad\quad \mathbf{g}_\ell^i \longleftarrow \mathbf{g}_\ell^{i-1} + \zeta^i \mathbf{d}_1^i$
18 $\quad\quad \mathbf{r}_\ell^i \longleftarrow \mathbf{r}_\ell^{i-1} - \zeta^i \boldsymbol{\mathcal{V}}^i$
19 $\quad i \longleftarrow i + 1$

D. Serial/Parallel Interference Cancellation Architecture

In this section, we introduce a modified SIC architecture operating at the receiver. The proposed structure consists of a PIC unit within each successive step. The main idea is to exploit the approximated equalization vectors of each stage, which have been obtained by the GP, in order to cancel out all the remaining interference of the adjacent subcarriers. Potentially, this structure could remove the entire interference at each stage, thus avoiding the ordering step.

The proposed SIC/PIC equalizer, termed as *Forward OSIC* (FOSIC), is composed by N stages, where the ordering of each stage is defined by $z_k \in [1, N]$. The functional block of the kth stage is depicted in Fig. 3. It is composed by the following basic units.

1) equalizer computation;
2) channel estimation;
3) forward ICI cancellation;
4) ordering update, and;
5) current ICI cancelation unit.

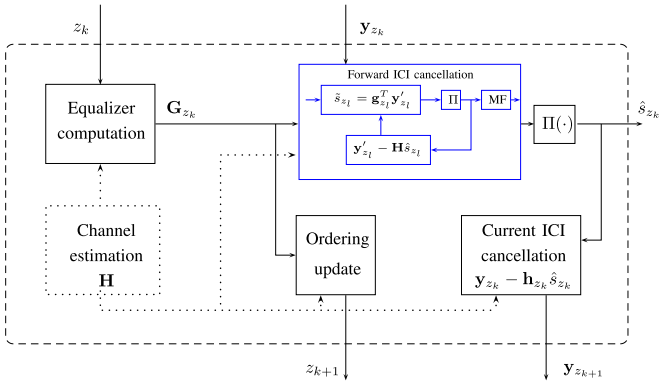

Fig. 3. FOSIC block model for the z_kth stage of the proposed equalizer. The part in blue cancels the ICI caused due to the subsequent symbols.

The outputs are the estimated symbol $\hat{s}_{z_k}$, the index z_{k+1} of the symbol to be detected at the next stage, and the updated input stream $\mathbf{y}_{z_k}$. In the following part of this section, we focus on each one of the building units separately.

The equalizer computation unit employs the proposed low-complexity algorithm. This will provide us the equalization vectors for the remaining adjacent subcarriers, i.e., $\mathbf{g}_l, l \in [k+1, \ldots, N]$.

The operation of channel estimation unit, which is depicted with dotted line, is out of the scope of this paper; a detailed review regarding efficient estimation schemes for doubly selective channels may be found in [12], [35], and [36].

The operation of the PIC unit removes the ICI caused by the undetected symbols of the remaining subcarriers from the input stream $\mathbf{y}_k$, while the ICI caused by the previously detected symbols has been removed from the previous stages. Assuming that the symbol decisions are correct, i.e., $\hat{s}_k = s_k, k \in [1, \ldots, N]$, then at the output, the updated input signal has no remaining ICI. Therefore, the updated input stream $\mathbf{y}'_N$ can be expressed as

$$\mathbf{y}'_N = \mathbf{h}_k s_k + \mathbf{w}. \tag{24}$$

Note that the MMSE equalizer essentially becomes the *matched filter* [13] for the input $\mathbf{y}'_N$. The equalization vector of the kth stage may be written as

$$\mathbf{g}_k^T = (\mathbf{h}_k^H \mathbf{h}_k + \sigma^2 \mathbf{I})^{-1} \mathbf{h}_k^H = \frac{1}{\sigma^2 + \|\mathbf{h}_k\|_2^2} \mathbf{h}_k^H. \tag{25}$$

The updated input vector for the current stage k, can be expressed as $\mathbf{y}'_N = \mathbf{y} - \sum_{m=1, m\neq k}^{N} \mathbf{H}_m s_m$, and thus, the current symbol can be estimated as follows:

$$\tilde{s}_k = \mathbf{g}_k^T \mathbf{y}'_N = \frac{\mathbf{h}_k^H \mathbf{y}'_N}{\sigma^2 + \|\mathbf{h}_k\|_2^2}. \tag{26}$$

The decision of the current symbol, and hence, the output of the kth stage is

$$\hat{s}_k = \Pi(\tilde{s}_k). \tag{27}$$

Finally, the current ICI cancellation unit is employed in order to remove the currently detected symbol from the input stream $\mathbf{y}_k$ according to

$$\mathbf{y}_{k+1} = \mathbf{y}_k - \mathbf{h}_k \hat{s}_k. \tag{28}$$

Then $\mathbf{y}_{k+1}$ is forwarded to the next stage.

IV. Computational Complexity

In this section, we provide a detailed description of the complexities required by the presented schemes, in terms of floating-point operations (FLOP). The complexity of the OSIC equalizer $\mathcal{C}^{\text{osic}}$ consists mainly of the cost of autocorrelation matrix computation/update, the solution of the linear system with multiple RHS and the ordering cost, i.e.,

$$\mathcal{C}^{\text{osic}} = \mathcal{C}^{\text{osic}}_{\text{update}} + \mathcal{C}^{\text{osic}}_{\text{inversion}} + \mathcal{C}^{\text{osic}}_{\text{ordering.}} \tag{29}$$

Specifically, considering the first term of this sum, we have that

$$\mathcal{C}^{\text{osic}}_{\text{update}} = \sum_{k=0}^{N-1} \left\{ N(N-k)^2 + \frac{(N-k)(N+k)}{2} + \frac{N-k}{2} \right\} \tag{30}$$

$$= \frac{1}{6} N(2N^3 + 5N^2 + 4N + 1) \text{ FLOPs}. \tag{31}$$

FLOP counts for the Gram matrix $\mathbf{H}_k^H \mathbf{H}_k$ computation, with $\mathbf{H}_k \in \mathbb{C}^{N \times N-k}$, is equal to $N(N-k)^2 + (N-k)(N - \frac{N-k}{2}) - \frac{N-k}{2}$.

Considering now $\mathcal{C}^{\text{osic}}_{\text{inversion}}$ and assuming that the inversion of a Hermitian matrix is obtained via Cholesky (LDL) decomposition, we have that $\mathcal{C}^{\text{osic}}_{\text{inversion}} = \frac{1}{6} N(5N^3 + 13N^2 + 4N + 2)$ FLOPs. The cost of the ordering based on the maximum SINR is $\mathcal{C}^{\text{osic}}_{\text{ordering}} = \frac{1}{6} N(4N^3 + 3N^2 - N)$ FLOPs. Therefore, the total complexity is $\mathcal{C}^{\text{osic}} = \frac{1}{6} N(11N^3 + 21N^2 + 7N + 3)$ FLOPs.

Let us now proceed with some analysis regarding the computational complexity of the proposed single-seed algorithm. For this, we can decompose the costs into the following operations.

1) computation of the autocorrelation matrix $\frac{3N^3}{2} + \frac{N^2}{2} - \frac{N}{2}$ FLOPs;
2) Hermitian matrix-vector multiplication $\mathbf{A}_{z_k} \mathbf{d}_k^i \forall k \in [0, N-1]$ and $i \in [1, I_k]$ in the CG procedure

$$\mathcal{C}_{\text{cg}} = \sum_{k=0}^{N-1} \sum_{i=1}^{I_k} \left\{ N^2 - \frac{N}{2} \right\}; \quad \text{and} \tag{32}$$

3) matrix-vector multiplication in the GP procedure

$$\mathcal{C}_{\text{gp}} = \sum_{k=0}^{N-2} \sum_{i=1}^{I_k} \{2N(N-k-1) - (N-k-1)\}. \tag{33}$$

Let $\bar{I}$ denotes the average number of iterations, which are required for convergence of the CG algorithm per stage. Then, the complexity costs (32) and (33) can be approximated as

$$\mathcal{C}^{\text{av}}_{\text{cg}} = \bar{I} \sum_{k=0}^{N-1} \left\{ N^2 - \frac{N}{2} \right\} = \bar{I} \left(N^3 - \frac{N^2}{2} \right) \text{ FLOPs} \tag{34}$$

TABLE II
COMPLEXITY OF BLOCK OSIC, NONBANDED EQUALIZERS

Method		Complexity (FLOPs)
Conventional technique [12]	via Gaussian elimination	$\frac{1}{6}N(11N^3+21N^2+7N+3)$
	via LDL	$\frac{1}{6}N(7N^3+18N^2+8N+3)$
Proposed algorithm (OSIC)	w.r.t. $\bar{I}$ (mean # iterations)	$\bar{I}\left(\frac{1}{2}N(1-2N)^2\right)+\frac{3N^3}{2}+\frac{N^2}{2}-\frac{N}{2}$
	worst case scenario	$\frac{1}{6}N\left(7N^3+\frac{17}{2}N^2-\frac{5}{2}N-1\right)$
Proposed algorithm (FOSIC)	worst case scenario	$\frac{1}{6}N\left(7N^3+\frac{29}{2}N^2+\frac{N}{2}-4\right)$

and

$$\mathcal{C}_{\text{gp}}^{\text{av}} = \bar{I}\sum_{k=0}^{N-2}\{2N(N-k-1)-(N-k-1)\} \quad (35)$$

$$= \bar{I}\frac{1}{2}\left(N(2N-1)(N-1)\right) \text{ FLOPs.} \quad (36)$$

1) Worst-Case Scenario: In the worst case, the number of the required iterations I_k for convergence of the CG algorithm at each stage is $I_k = N-k$. In that case, the complexity of the proposed single-seed algorithm is equal to $\mathcal{C}_{\text{cg-gp}}^{w} = \frac{1}{12}N\left(14N^3+17N^2-5N-2\right)$ FLOPs. It is obvious that $\mathcal{C}_{\text{cg-gp}} \leq \mathcal{C}_{\text{conv}}$, i.e., the complexity of the proposed technique (single-seed version) will be always lower than the conventional one.

2) FOSIC Complexity: The proposed FOSIC architecture exploits the already known equalization vectors of each stage, in order to remove the remaining ICI through tentative decisions. The additional cost over OSIC complexity, is for the computation of the tentative symbol decisions, which is given by: $\mathcal{C}_{\text{fosic}} = \sum_{k=0}^{N-1}\{2N(N-k)-(N-k)\} = N^2 2N-1)$, and thus, we conclude that OSIC and FOSIC architectures have the same complexity order.

In Table II, we summarize the computational complexity for the conventional technique and the proposed one in terms of FLOPs.

V. SIMULATION RESULTS

In this section, the performance of the proposed equalizer is experimentally evaluated via extensive simulations.

A. Setup

The simulations were performed with machine precision 10^{-16} and the number of Monte Carlo realizations was at least 10^3. Furthermore, we have made the assumptions of full channel state information and perfect carrier and phase synchronization.

The general setup includes the simulation of an OFDM system that operates over a doubly selective channel. The basic parameters for the simulation experiments are shown in Table III. For the channel modeling, we have adopted the WSSUS fading model with a 3-tap exponential delay power profile, given by

TABLE III
BASIC PARAMETERS FOR SIMULATION EXPERIMENTS

Parameter	Value
Modulation mode	4 QAM, 16 QAM
Number of subcarriers	$N = 32$
FFT length	32
Cyclic prefix length	$N_{\text{cp}} = 3$
Channel length	$L = 3$

$$\sigma_h^2(l) = \frac{e^{-l/L}}{\sum_{m=0}^{L-1} e^{-m/L}}, \quad \text{for } l = 0,1,\ldots,L-1 \quad (37)$$

where $L = 3$. Each channel tap is a complex Gaussian random process independently generated with the Doppler spectrum based on the Jakes' model [37]. The autocorrelation function of each channel tap is equal to the zerothorder Bessel function of the first kind, i.e., $r_t(\Delta t) = J_0(2\pi f_d \Delta t)$, where $\Delta t \in [-N, N] \subset \mathbb{Z}$ and f_d is the normalized Doppler spread defined as $f_d \triangleq \frac{1}{F}\frac{f_c v}{c}$, where v is the vehicle relative velocity, f_c is the carrier frequency, F is the subcarrier separation, and c is the speed of light. In this paper, we have adopted the normalization over the signaling rate [14], i.e., $F = N$.

To evaluate the performance of the proposed equalizer, several techniques from the literature of ICI mitigation have been employed. In particular, as the best one in terms of BER performance we have used the equalizer of [12] (termed as *block OSIC, nonbanded*), while as a low-complexity technique we have used the equalizer of [38] (termed as *block MMSE, banded windowed*).

It is important to mention here that, in the case of banded-windowed equalization, the soft decision is given by

$$\tilde{\mathbf{x}}_{\mathbf{w}} = \mathbf{H}_K^H\left(\mathbf{H}_K\mathbf{H}_K^H + \frac{\sigma_z^2}{\gamma}\mathcal{C}(\mathbf{w})\mathcal{C}(\mathbf{w})^H\right)^{-1}\mathbf{y}_{\mathbf{w}} \quad (38)$$

where $\mathbf{H}_K$ is the K-banded approximation of the frequency-domain channel matrix, i.e., $\mathbf{H}_K = \mathbf{E}_K \circ \mathbf{H}$. The parameter $\gamma \in (0,1]$ is the regularization parameter and $\mathbf{w}$ is the window applied to the received symbol $\mathbf{y}$, with $\mathbf{y}_{\mathbf{w}} \triangleq \mathcal{C}(\mathbf{w})\mathbf{y}$. The design of the window was based on the maximum SINR criterion [14].

Additionally, as an alternative to block equalization, we have used the serial equalizer of [13] (termed as *serial DFE*). The

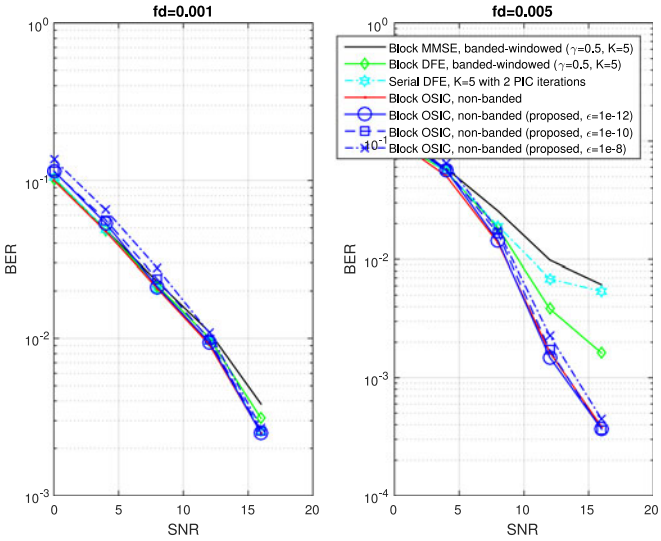

Fig. 4. BER comparison w.r.t. SNR for low Doppler spread and 4 QAM.

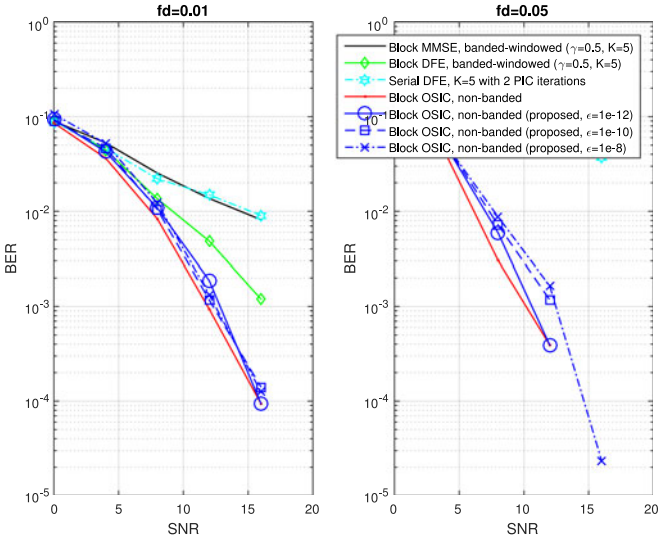

Fig. 5. BER comparison w.r.t. SNR for medium Doppler spread and 4 QAM.

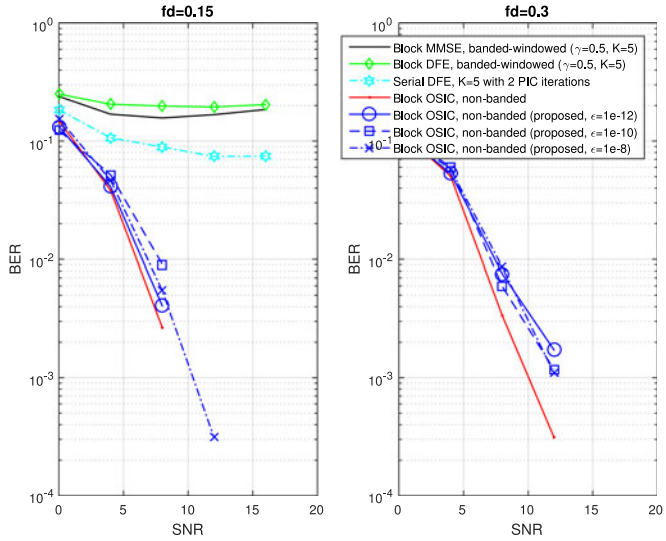

Fig. 6. BER comparison w.r.t. SNR for high Doppler spread and 4 QAM.

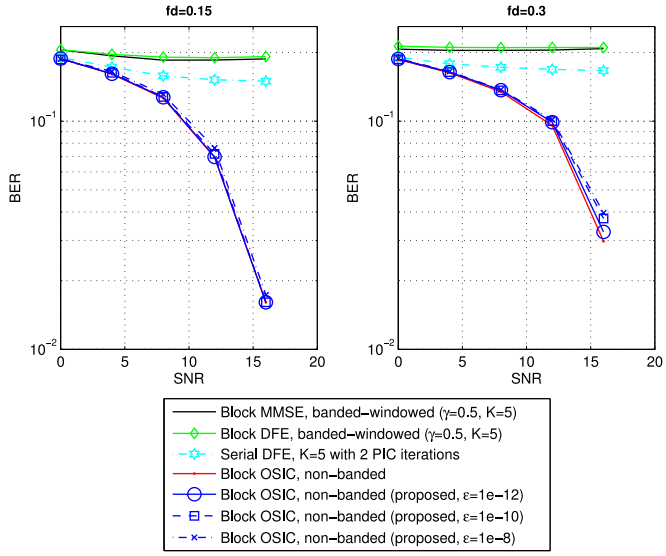

Fig. 7. BER comparison w.r.t. SNR: 16 QAM.

number of subcarriers that are processed at each step is equal to K. Another important characteristic of the technique in [13] is the PIC operation that is employed at the output of the equalizer, where the number of the PIC iterations determines the complexity/performance tradeoff of the technique.

B. BER Performance

In Figs. 4–6, the BER of 4 QAM modulation w.r.t. SNR is shown, for different values of normalized Doppler frequency f_d. We can observe that, for very low Doppler spreads ($f_d < 0.005$), all the techniques have about the same performance. For higher Doppler spreads, the banded and the serial approximation techniques suffer from severe ICI, while the value of K has great impact at their performance. For $f_d \leq 0.1$, the block DFE technique [39] exhibits BER performance close to the OSIC (see Fig. 5), while for higher Doppler spreads, K must be also increased in order to retain this performance. On the contrary, the OSIC techniques are able to mitigate effectively the ICI under all Doppler spread cases. The BER of the proposed technique approximates closely that of the block OSIC nonbanded equalizer [12], depending on the parameter ϵ. In addition, note that, the performance of the proposed equalizer for the larger error tolerance case, i.e., $\epsilon = 10^8$, does not depend on the different values of the normalized Doppler frequency f_d.

The application of OSIC architecture is significantly favored for the 16 QAM case, with the normalized Doppler frequency set to $f_d = 0.3$. As it is shown in Fig. 7, the banded and serial equalizers seem to be totally ineffective.

In Fig. 8, we show the mean-square error (MSE) of the proposed FOSIC architecture w.r.t. the SNR for $f_d = 0.3$. We consider multiple- and single-seed versions with $\epsilon = 10^{-12}$ and $\epsilon = 10^{-8}$, respectively. The proposed FOSIC architecture with the multiseed algorithm has the lowest MSE, along with the single-seed version for SNR > 8. The performance gains of the proposed structure seem to be significant at the high SNR

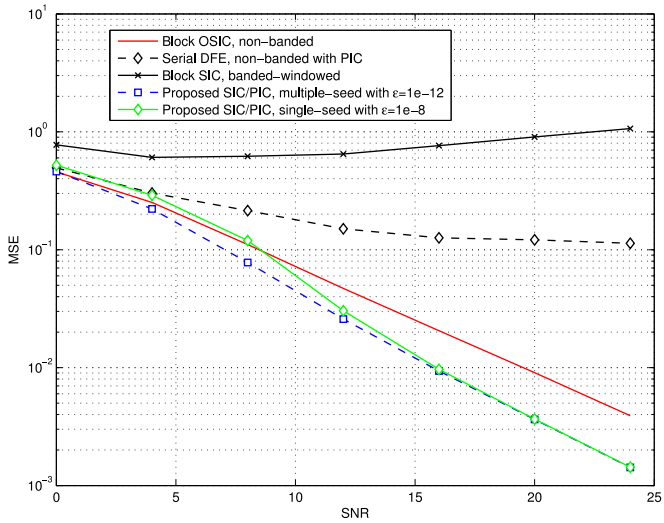

Fig. 8. Evaluation of FOSIC (PIC/SIC) architecture in terms of MSE w.r.t. SNR.

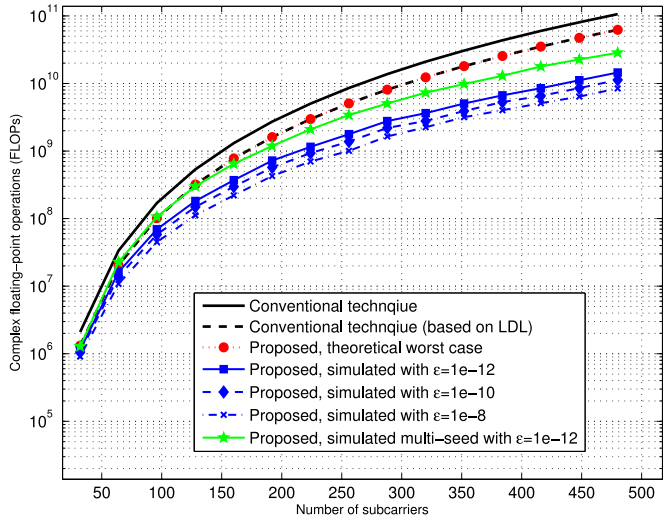

Fig. 9. Complexity w.r.t. the number of subcarriers, SNR $= 15$ dB, and $L = 3$.

TABLE IV
COMPARISON OF THE COMPUTATIONAL COMPLEXITY ORDER

Equalizer	Complexity
Proposed schemes (CG-GP {F}OSIC)	$\mathcal{O}(N^3\bar{I})$
nonbanded OSIC (Choi *et al.* [12])	$\mathcal{O}(N^4)$
DFE with K taps (Cai *et al.* [13])	$\mathcal{O}(N^2K)$
banded MMSE-BDFE windowing (Rugini *et al.* [38])	$\mathcal{O}(NK^2)$

regimes, where there is small error propagation due to incorrect symbol detection. Also note that, the block SIC is banded and windowed according to the maximum SINR criterion [14], while the serial DFE [13] has a PIC operation after the DFE, performing three iterations. Note that the MSE of the block SIC increases along with the SNR, which is due to the bad condition of the equalization matrix.

C. Complexity

Let us now examine the performance of the proposed iterative algorithm in terms of computational complexity. In Table IV, the complexity order of the employed techniques is shown. Note that, $\bar{I}$ denotes the mean iterations number required for the convergence of the proposed iterative algorithm.

In Fig. 9 the complexity of the proposed algorithms is shown w.r.t. the number of the subcarriers. The complexity is expressed in terms of complex FOP. For reference, we also show the complexity of the conventional technique, when computed either via the Gaussian elimination or via the LDL factorization. For the proposed algorithms we show the worst case scenario and the average case, where $\bar{I}$ is the average number of iterations. Note that, the average number of required iterations for the convergence of the CG algorithm, i.e., $\bar{I}$, is a function of the parameter ϵ, as it can be shown in Fig. 9. Additionally, we plot the complexity of the multiple-seed version of the algorithm.

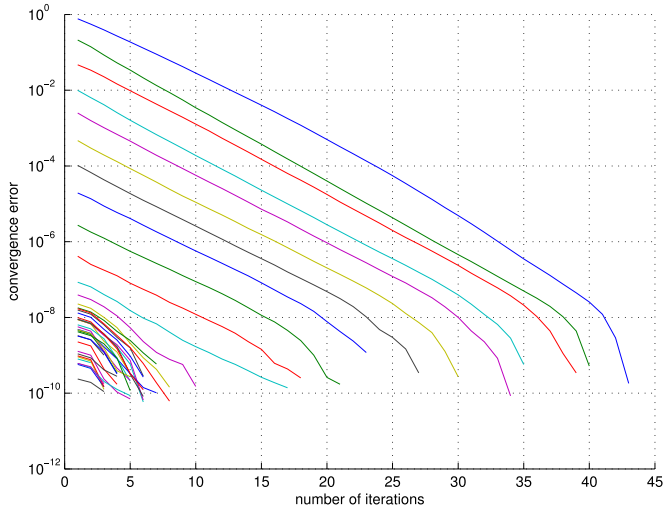

Fig. 10. Convergence rate of CG-GP algorithm for all 48 subcarriers at the z_1 OSIC stage.

Based on the complexity curves, we confirm that the proposed algorithms practically have lower complexity cost than the conventional technique. The multiple-seed version (with $\epsilon = 10^{-12}$) has the lowest complexity gain and hence almost zero reconstruction error. The single-seed version has considerable complexity gains, depending on the ϵ. Even for the case of $\epsilon = 10^{-12}$, the complexity drops an order of magnitude for large OFDM blocks.

D. Convergence

In the following, we investigate the convergence rate of the seed and the nonseed systems. More precisely, we verify the fast convergence rate of the systems due to the initialization based on GP, and thus the reduction of the system's size through the OSIC architecture. In Fig. 10, the convergence curves of the proposed algorithm at the first OSIC stage are depicted; each curve,

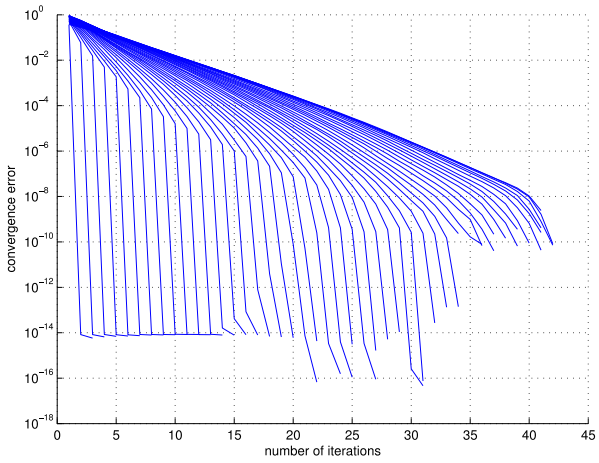

Fig. 11. Convergence rate of CG-GP algorithm of the first subcarrier at the 2–48 OSIC stages.

indexed with the variable l, represents the squared norm of the estimation absolute error $\|\mathbf{g}_{1,l} - \mathbf{g}_{1,l}^{\star}\|^2, l = 1, \ldots, N$, with respect to the CG iteration number, where $\mathbf{g}_{1,l}$ is the approximated equalization vector of the first OSIC stage for the lth subcarrier, while $\mathbf{g}_{1,l}^{\star}$ is its optimum value. The SNR for this experiment was set to 15 dB, while the error tolerance to 10^{-8}.

The top curve in Fig. 10 shows the convergence of the first subcarrier at the first stage. It requires up to N iterations to converge to the solution $\mathbf{g}_{1,1}$, since no initialization is employed. For the next subcarriers, due to the GP, there is a significant increase in the convergence rate. Indeed, concerning the seventh subcarrier, the error $\|\mathbf{g}_{1,7} - \mathbf{g}_{1,7}^{\star}\|^2$ begins from 10^{-4}, which verifies the fact that the projections-based initialization vector is essentially the solution vector for the majority of the subcarriers.

In Fig. 11, the convergence curves of the proposed algorithm at the second–48th OSIC stages are depicted; each curve, indexed with the variable k, represents the estimation's absolute error $\|\mathbf{g}_{k,1} - \mathbf{g}_{k,1}^{\star}\|, k = 1, \ldots, N$, with respect to the CG iteration number. As the OSIC stage increases, the first subcarrier of each stage exhibits faster convergence rate. Recall that in the OSIC architecture, the linear system dimensions are reduced at each successive stage. This process also reduces the eigendimensions of the system that results into increase of the convergence speed of the proposed iterative algorithm, since the convergence rate of the CG algorithm is strongly related with the number of the distinct eigenvalues.

VI. Conclusion

In this paper, we introduced an OSIC-based interference cancellation scheme for OFDM systems operating over doubly selective channels. The key feature of this architecture is that it removes the ICI caused by both the previously detected symbols and the forward ones, which are temporally detected at each stage. To estimate efficiently the equalizer filters, a CG-based method that applies GP for the initialization of the filters has been proposed, accelerating the convergence rate of the algorithm. Different initialization schemes were evaluated in terms of both performance and complexity. The proposed scheme has been tested via simulations, assuming a practical communication scenarios with high Doppler delay spreads. The experimental results showed that the proposed equalizer achieves lower BER values than the existing nonbanded ICI cancellation schemes at a lower computational cost.

References

[1] F. Hlawatsch and G. Matz, *Wireless Communications Over Rapidly Time-Varying Channels*, 1st ed. New York, NY, USA: Academic, 2011.
[2] B. Stantchev and G. Fettweis, "Time-variant distortions in OFDM," *IEEE Commun. Lett.*, vol. 4, no. 10, pp. 312–314, Oct. 2000.
[3] T. Wang, J. Proakis, E. Masry, and J. Zeidler, "Performance degradation of OFDM systems due to Doppler spreading," *IEEE Trans. Wireless Commun.*, vol. 5, no. 6, pp. 1422–1432, Jun. 2006.
[4] P. Robertson and S. Kaiser, "The effects of Doppler spreads in OFDM(A) mobile radio systems," in *Proc. IEEE 58th Veh. Technol. Conf.*, 1999, vol. 1, pp. 329–333.
[5] *Part 11: Wireless LAN Medium Access Control (MAC) and Physical Layer (PHY) Specifications Amendment 6: Wireless Access in Vehicular Environments*, IEEE Std. 802.11p, Jul. 2011.
[6] R1-070674, "LTE physical layer framework for performance verification," 3GPP TSG RAN1 48, Feb. 2007.
[7] *Part 16: Air Interface for Fixed and Mobile Broadband Wireless Access Systems*, IEEE Std. 802.16e, 2006.
[8] *Digital Video Broadcasting (DVB): Transmission System for Hand-Held Terminals (DVB-H),* ETSI, EN 302 304 V1.1.1, Nov. 2004.
[9] S. Rangan, T. Rappaport, and E. Erkip, "Millimeter-wave cellular wireless networks: Potentials and challenges," *Proc. IEEE*, vol. 102, no. 3, pp. 366–385, Mar. 2014.
[10] W. G. Jeon, K. H. Chang, and Y. S. Cho, "An equalization technique for orthogonal frequency-division multiplexing systems in time-variant multipath channels," *IEEE Trans. Commun.*, vol. 47, no. 1, pp. 27–32, Jan. 1999.
[11] A. Stamoulis, S. Diggavi, and N. Al-Dhahir, "Intercarrier interference in MIMO OFDM," *IEEE Trans. Signal Process.*, vol. 50, no. 10, pp. 2451–2464, Oct. 2002.
[12] Y. S. Choi, P. J. Voltz, and F. A. Cassara, "On channel estimation and detection for multicarrier signals in fast and selective Rayleigh fading channels," *IEEE Trans. Commun.*, vol. 49, no. 8, pp. 1375–1387, Aug. 2001.
[13] X. Cai and G. Giannakis, "Bounding performance and suppressing intercarrier interference in wireless mobile OFDM," *IEEE Trans. Commun.*, vol. 51, no. 12, pp. 2047–2056, Dec. 2003.
[14] P. Schniter, "Low-complexity equalization of OFDM in doubly selective channels," *IEEE Trans. Signal Process.*, vol. 52, no. 4, pp. 1002–1011, Apr. 2004.
[15] S. U. Hwang, H. J. Lee, and J. Seo, "Low complexity iterative ICI cancellation and equalization for OFDM systems over doubly selective channels," *IEEE Trans. Broadcast.*, vol. 55, no. 1, pp. 132–139, Mar. 2009.
[16] E. Vlachos, A. Lalos, and K. Berberidis, "Galerkin projections-based ICI cancellation in OFDM systems with doubly selective channels," in *Proc. 18th Int. Conf. Digit. Signal Process.*, Jul. 2013, pp. 1–6.
[17] E. Vlachos, A. Lalos, and K. Berberidis, "Regularized MMSE ICI equalization for OFDM systems over doubly selective channels," in *Proc. IEEE Int. Symp. Signal Process. Inform. Technol.*, Dec. 2013, pp. 458–463.
[18] K. Fang, L. Rugini, and G. Leus, "Low-complexity block turbo equalization for OFDM systems in time-varying channels," *IEEE Trans. Signal Process.*, vol. 56, no. 11, pp. 5555–5566, Nov. 2008.
[19] T. Hrycak and G. Matz, "Low-complexity time-domain ICI equalization for OFDM communications over rapidly varying channels," in *Proc. 14th Asilomar Conf. Signals, Syst., Comput.*, vol. 29, no. 1, Nov. 2006, pp. 1767–1771.
[20] G. Taubock, M. Hampejs, P. Svac, G. Matz, F. Hlawatsch, and K. Grochenig, "Low-complexity ICI/ISI equalization in doubly dispersive multicarrier systems using a decision-feedback LSQR algorithm," *IEEE Trans. Signal Process.*, vol. 59, no. 5, pp. 2432–2436, May 2011.
[21] J. Tong and P. Schreier, "Regularized preconditioning for Krylov subspace equalization of OFDM systems over doubly selective channels," *IEEE Wireless Commun. Lett.*, vol. 2, no. 4, pp. 367–370, Aug. 2013.

[22] Z. Tang, R. Remis, and M. Nordenvaad, "On preconditioned conjugate gradient method for time-varying OFDM channel equalization," in *Proc. IEEE Int. Conf. Acoust., Speech Signal Process.*, Mar. 2012, pp. 3197–3200.
[23] T. F. Chan and W. L. Wan, "Analysis of projection methods for solving linear systems with multiple right-hand sides," *SIAM J. Sci. Comput.*, vol. 18, no. 6, pp. 1698–1721, Nov. 1997.
[24] T. Zemen, L. Bernado, N. Czink, and A. Molisch, "Iterative time-variant channel estimation for 802.11p using generalized discrete prolate spheroidal sequences," *IEEE Trans. Veh. Technol.*, vol. 61, no. 3, pp. 1222–1233, Mar. 2012.
[25] M. Ashour, A. Attia, A. ElMoslimany, Y. Mohasseb, and A. El-Keyi, "MIMO vehicle to vehicle channels: An experimental study," in *Proc. IEEE 80th Veh. Technol. Conf.*, Sep. 2014, pp. 1–5.
[26] P. Bello, "Characterization of randomly time-variant linear channels," *IEEE Trans. Commun. Syst.*, vol. CS-11, no. 4, pp. 360–393, Dec. 1963.
[27] A. Lozano and C. Papadias, "Layered space-time receivers for frequency-selective wireless channels," *IEEE Trans. Commun.*, vol. 50, no. 1, pp. 65–73, Jan. 2002.
[28] P. W. Wolniansky, G. J. Foschini, G. D. Golden, and R. A. Valenzuela, "V-BLAST: An architecture for realizing very high data rates over the rich-scattering wireless channel," in *Proc. URSI Int. Symp. Signal, Syst., Electron*, 1998, pp. 295–300.
[29] S. Diggavi, "Analysis of multicarrier transmission in time-varying channels," in *Proc. IEEE Int. Conf. Commun.*, vol. 3, Jun. 1997, pp. 1191–1195.
[30] H. A. V. D. Vorst, *Iterative Krylov Methods for Large Linear Systems*. Cambridge, U.K.: Cambridge Univ. Press, 2003.
[31] O. Axelsson, *Solution of Linear Systems of Equations: Iterative Methods*. New York, NY, USA: Springer-Verlag, 1977.
[32] C. C. Paige and M. A. Saunders, "LSQR: An algorithm for sparse linear equations and sparse least squares," *ACM Trans. Math. Softw.*, vol. 8, no. 1, pp. 43–71, Mar. 1982.
[33] T. F. Chan and M. K. Ng, "Galerkin projection methods for solving multiple linear systems," *SIAM J. Sci. Comput.*, vol. 21, no. 3, pp. 836–850, Nov. 1999.
[34] A. S. Lalos, V. Kekatos, and K. Berberidis, "Adaptive conjugate gradient DFEs for wideband MIMO systems," *IEEE Trans. Signal Process.*, vol. 57, no. 6, pp. 2406–2412, Jun. 2009.
[35] S. Yameogo, J. Palicot, and L. Cariou, "Mobile radio channels' estimation for SC-FDMA systems by means of adequate noise and inter-carrier interference filtering in a transformed domain," in *Proc. IEEE GLOBECOM Workshops*, Dec. 2010, pp. 1302–1306.
[36] L. Zhang, Z. Hong, L. Thibault, R. Boudreau, and Y. WuIEEE, "A low-complexity robust OFDM receiver for fast fading channels," *IEEE Trans. Broadcast.*, vol. 60, no. 2, pp. 347–357, Jun. 2014.
[37] W. C. Jakes, *Microwave Mobile Channels*. New York, NY, USA: Wiley, 1974.
[38] L. Rugini, P. Banelli, and G. Leus, "Low-complexity banded equalizers for ofdm systems in doppler spread channels," *EURASIP J. Appl. Signal Process.*, vol. 2006, pp. 248–248, Jan. 2006.
[39] L. Rugini and P. Banelli, "Performance analysis of banded equalizers for OFDM systems in time-varying channels," in *Proc. IEEE 8th Workshop Signal Process. Adv. Wireless Commun.*, Jun. 2007, pp. 1–5.

Evangelos Vlachos received the Diploma degree in computer engineering and informatics, the Masters degree in signal processing systems, and the Ph.D. degree in signal processing for wireless communications from the University of Patras, Patras, Greece, in 2005, 2009, and 2015, respectively.

He is currently a Postdoctoral Researcher with the Signal Processing and Communications Laboratory. He has participated in several European projects related to wireless communications and signal processing (e.g., ENDECON, THERMOCAMERA, GRIC, HANDiCAMS).

Aris S. Lalos received the Diploma, M.A.Sc., and Ph.D. degrees in signal processing and communications from the Computer Engineering and Informatics Department (CEID), School of Engineering (SE), University of Patras (UoP), Patras, Greece, in 2003, 2005, and 2010, respectively.

From 2005 to 2010, he has been a Research Fellow with the Signal Processing and Communications Laboratory, CEID, SE, UoP, and was with Signal Theory and Communications, Department of the Technical University of Catalonia, Barcelona, Spain, from October 2012 to December 2014. From October 2011 to October 2012, he was a Telecommunication Research Engineer with Analogies S.A, which was an early stage start up. He is currently a Postdoctoral Researcher with the Visualization and Virtual Reality Group. He is an author of more than 44 research papers in 19 international journals, 22 conferences, and three edited books, and he acts as a Regular Reviewer for several technical journals.

Dr. Lalos received the Best Demo Award at the IEEE CAMAD Conference in 2014, the Best Paper Award at the IEEE ISSPIT Conference in 2015, and in January 2015, he was nominated as Exemplary Reviewer for the IEEE COMMUNICATIONS LETTERS.

Kostas Berberidis (S'87–M'90–SM'07) received the Diploma degree in electrical engineering from Democritus University of Thrace, Komotini, Greece, in 1985 and the Ph.D. degree in signal processing and communications from the University of Patras, Patras, Greece, in 1990.

During 1991, he was with the Signal Processing Laboratory, National Defense Research Center, Greece. From 1992 to 1994 and from 1996 to 1997, he was a Researcher with the Computer Technology Institute, Patras, Greece. During 1994–1995, he was a Postdoctoral Fellow with CCETT/CNET, Rennes, France. Since December 1997, he has been with the Computer Engineering and Informatics Department, University of Patras, where he is currently a Professor and the Head of the Signal Processing and Communications Laboratory. Since 2008, he has been the Director of the SPCOM Research Unit of the Computer Technology Institute and Press "Diophantus." His research interests include adaptive signal processing, distributed processing and learning, signal processing for communications, and wireless sensor networks.

Prof. Berberidis has served or has been serving as a Member of scientific and organizing committees of several international conferences, as Associate Editor of the IEEE TRANSACTIONS ON SIGNAL PROCESSING and the IEEE SIGNAL PROCESSING LETTERS, and as a Guest Editor and Associate Editor of the of the EURASIP *Journal on Advances in Signal Processing*. Since February 2010, he has been serving as the Chair of the Greece Chapter of the IEEE Signal Processing Society. He is also currently a Member of two IEEE Technical Committees (SPTM and SPCE) and a Member of two EURASIP Special Area Teams (TMTSP and SPMuS). He is a Member of the Technical Chamber of Greece and a Member of EURASIP.